Human Molecular Genetics, 2020, Vol. 29, No. 10 1648–1657

doi: 10.1093/hmg/ddaa064
Advance Access Publication Date: 09 April 2020
General Article

GENERAL ARTICLE

Otx2b mutant zebrafish have pituitary, eye and mandible defects that model mammalian disease

Hironori Bando[1], Peter Gergics[1,†], Brenda L. Bohnsack[2], Kevin P. Toolan[1], Catherine E. Richter[3], Jordan A. Shavit[3] and Sally A. Camper[1,*]

[1]Department of Human Genetics, University of Michigan, Ann Arbor, MI 48109, USA, [2]Department of Ophthalmology and Visual Sciences, Kellogg Eye Center, University of Michigan, Ann Arbor, MI 48109, USA and [3]Division of Pediatric Hematology/Oncology, Department of Pediatrics, University of Michigan, Ann Arbor, MI 48109, USA

*To whom correspondence should be addressed at: Department of Human Genetics, University of Michigan Medical School, 5704 Medical Science Building II, 1301 Catherine St, Ann Arbor, MI 48109, USA. Tel: +1 7347630682; Email: scamper@med.umich.edu

Abstract

Combined pituitary hormone deficiency (CPHD) is a genetically heterogeneous disorder caused by mutations in over 30 genes. The loss-of-function mutations in many of these genes, including orthodenticle homeobox 2 (OTX2), can present with a broad range of clinical symptoms, which provides a challenge for predicting phenotype from genotype. Another challenge in human genetics is functional evaluation of rare genetic variants that are predicted to be deleterious. Zebrafish are an excellent vertebrate model for evaluating gene function and disease pathogenesis, especially because large numbers of progeny can be obtained, overcoming the challenge of individual variation. To clarify the utility of zebrafish for the analysis of CPHD-related genes, we analyzed the effect of OTX2 loss of function in zebrafish. The *otx2b* gene is expressed in the developing hypothalamus, and *otx2b*$^{hu3625/hu3625}$ fish exhibit multiple defects in the development of head structures and are not viable past 10 days post fertilization (dpf). *Otx2b*$^{hu3625/hu3625}$ fish have a small hypothalamus and low expression of pituitary growth hormone and prolactin (*prl*). The gills of *otx2b*$^{hu3625/hu3625}$ fish have weak sodium influx, consistent with the role of prolactin in osmoregulation. The *otx2b*$^{hu3625/hu3625}$ eyes are microphthalmic with colobomas, which may underlie the inability of the mutant fish to find food. The small pituitary and eyes are associated with reduced cell proliferation and increased apoptosis evident at 3 and 5 dpf, respectively. These observations establish the zebrafish as a useful tool for the analysis of CPHD genes with variable and complex phenotypes.

Introduction

Orthodenticle homeobox 2 (*Otx2*) is a homeobox gene with an essential role in the development of several craniofacial structures including the eye, jaw, and pituitary gland. It is expressed in the epiblast, anterior visceral endoderm, anterior definitive endoderm, and anterior neuroectoderm before and during gastrulation, and is involved in the patterning of the midbrain and forebrain (1). In humans, whole gene deletions and mutations in humans is likely caused by variation in other genes that enhance or suppress the phenotype (7).

Rodent models are costly for the analysis of genes like *Otx2* that exhibit incomplete penetrance and highly variable phenotype. This is especially true with *Otx2* because neonatal lethality necessitates the utilization of large numbers of pregnant females to obtain sufficient numbers of embryos for quantitative analysis. Conversely, hundreds of fertilized

[†]Present address: St. Joseph Mercy Hospital, Ann Arbor, MI 48106, USA.

Received: January 9, 2020. **Revised:** February 29, 2020. **Accepted:** March 30, 2020

eggs can be obtained from one zebrafish female in a single spawning, facilitating the analysis of variable phenotypes by increasing the sample size. A few zebrafish studies have been reported with human CPHD-related gene mutants and morphants. These include *fibroblast growth factor 3 (fgf3)* (8), *shh* (9), *gli1/2* (10), *pitx3* (11) and *pit1* (12). In some cases, pituitary and eye function were incompletely characterized, leaving it unclear whether the zebrafish is a reliable model for human CPHD-disease pathogenesis. Morpholino oligonucleotide (MO)-mediated knockdown of *otx2b* had variable, modest effects in zebrafish, although there was evidence that decreased *otx2b* exacerbated the effects of knockdown of other genes involved in head development such as *pgap1*, *msx1* and *prrx1* (2). Studies utilizing MO knockdown can be problematic because of off-target effects, the hypomorphic nature of the model, the retention of maternal mRNA, and the variability associated with microinjection (13). The use of genetically modified zebrafish can overcome these problems.

Here we report defects in the pituitary glands, mandibles and eyes of *otx2b* mutant fish that model the features of patients with *OTX2* mutations. The results suggest that *otx2b* deficiency causes reduced cell proliferation and increased apoptosis, resulting in organ hypoplasia. In addition, the eye and pituitary hormone deficiencies likely cause the early death of *otx2b* mutant zebrafish.

Results

otx2b $^{hu3625/hu3625}$ fish die between 11 and 12 days post fertilization (dpf)

In zebrafish, like the majority of teleosts, 30–40% of the genome is duplicated. Genome duplication during evolution results in 2 orthologs of the *otx2* gene: *otx2a* and *otx2b*. These genes encode proteins with only 70% identical amino acids. Human and mouse OTX2 are identical, and they have 90% amino acid conservation with otx2b, but otx2a is more divergent. These data suggest that otx2b is the primary ortholog of mammalian OTX2. Therefore, we analyzed *otx2b* mutant fish.

Otx2b^{hu3625} fish, which were generated by ethyl-N-nitrosourea mutagenesis through the Zebrafish Mutation Project (Wellcome Sanger Institute) (14), carry an A to C point mutation in the essential splice acceptor site of intron 2 (c.250-2A > C) that is predicted to ablate splicing from exon 2 to exon 3 (Fig. 1A). Failure to splice is predicted to produce mRNA that would encode a truncated version of the protein, p.W85ter22, which is normally 289 amino acids. This A > C change generates a novel *Msp1* site that is useful for genotyping WT, heterozygous and homozygous mutant fish (Fig. 1B). The Mendelian distribution of genotypes was as expected (1:2:1) through 10 dpf. However, there was an absence of *otx2b*$^{hu3625/hu3625}$ fish at 13 dpf (Table 1) indicating that the homozygous mutants died between 11 and 12 dpf. The analysis of *otx2b* transcripts by reverse transcription-polymerase chain reaction (RT-PCR) in 5 dpf fish revealed reduction in transcripts spliced from exon 1 to exon 2 in *otx2b*$^{hu3625/hu3625}$ fish in contrast to *otx2b*$^{hu3625/+}$ and *otx2b*$^{+/+}$ fish (Fig. 1C). Further, although transcripts spliced from exon 2 to exon 3 were readily detectable in *otx2b*$^{hu3625/+}$ and *otx2b*$^{+/+}$ fish, none were detected in *otx2b*$^{hu3625/hu3625}$, suggesting that disruption of the splice site caused nonsense-mediated mRNA decay, as expected based on the position of the premature termination codon. Mutant mRNA degradation may be associated with the upregulation of paralogous genes as transcriptional genetic compensation (15). RT-PCR analysis revealed no change in the expression of *otx2a*, paralogue of *otx2b*, in either in *otx2b*$^{hu3625/+}$ or *otx2b*$^{hu3625/hu3625}$ (Fig. 1C).

otx2b $^{hu3625/hu3625}$ have diminished pituitary hormone expression

Human *OTX2* variants can be associated with GH deficiency and CPHD while heterozygous mouse mutants show missing or dysmorphic pituitary glands (16, 17). In zebrafish, pituitary progenitor cells in the hypophyseal placode are present by 19 h post fertilization (hpf) (18) and differentiate into prolactin (*prl*)-expressing cells by 1 dpf and growth hormone (*gh*)-expressing cells by 2 dpf. At 1 dpf, *otx2b*$^{hu3625/hu3625}$ embryos had decreased the expression of *lim homeobox protein 3 (lim3)* (65.6 ± 29.2% in contrast to wild type (WT), Fig. 2A and B), an early marker for pituitary progenitor cells suggesting poor commitment to pituitary cell fate. Further, differentiation into *prl* and *gh*-positive cells was assessed by *in situ* hybridization and quantification of the area of pituitary hormone expression. Hormone-expressing cells are clustered together in the zebrafish pituitary, and the *gh*- and *prl*-expressing cells have only 1 cluster (19). Thus, differentiation into these cell types can be assessed by carrying out *in situ* hybridization for pituitary hormone transcripts and quantifying the area of pituitary hormone expressing cells. The *prl*-expressing area in *otx2b*$^{hu3625/hu3625}$ mutants was significantly smaller in contrast WT and *otx2b*$^{hu3625/+}$ heterozygotes at 5 (73.8 ± 14.8% in contrast to WT) and 10 dpf (71.6 ± 12.4% in contrast to WT), but not at 1 and 3 dpf (Fig. 2C and D, Supplementary Fig. S1A–F). However, at these earlier time points small differences between genotypes may be obscured by the high intensity of *prl* expression. *prl* has an important role in osmoregulation via regulation of transcription of sodium transporters in the gills (20), and consistently 7 dpf *otx2b*$^{hu3625/hu3625}$ mutants showed weaker sodium accumulation in the gills than WT and heterozygotes (Fig. 2I and J). *In situ* hybridization also demonstrated that the *gh*-expressing area was significantly smaller at 3 (70.3 ± 18.7% in contrast to WT), 5 (72.1 ± 12.1% in contrast to WT) and 10 dpf (62.1 ± 14.1% in contrast to WT, Fig. 2E and F, Supplementary Fig. S1G–J). Despite the decrease in *gh*-expressing area, there was no difference in body length of the *otx2b*$^{hu3625/hu3625}$ larvae at 10 dpf (Fig. 1D and E). Thus, while *prl* deficiency in *otx2b*$^{hu3625/hu3625}$ mutants likely affects osmotic pressure homeostasis, decreased *gh* had no effect on larval growth prior to early lethality.

In mammals, *Otx2* is expressed in the forebrain, midbrain, cerebellum and retina. Further, expression is detected in the developing hypothalamus, but there is little or no expression within the pituitary (7, 21). In zebrafish, *in situ* hybridization showed that *otx2b* was expressed at the forebrain to midbrain-hindbrain boundary but not in the pituitary between 1 and 10 dpf (Supplementary Fig. S2A). Thus, the reduced commitment to pituitary fate and decreased *prl* and *gh* expression in *otx2b*$^{hu3625/hu3625}$ mutants must be indirect. Signals from the hypothalamus, such as *nk2 homeobox 4b (nkx2.4b)* and *fgf3*, are important for pituitary placode growth, and 1 dpf *otx2b*$^{hu3625/hu3625}$ mutants showed a smaller region of *nkx2.4b*-expression (78.9 ± 9.7% compared to WT) and slightly shorter length of the *fgf3*-positive region in the hypothalamus (86.6 ± 15.5% compared to WT) (Fig. 2G and H; Supplementary Fig. S2B). This suggests that *otx2b* expression in the hypothalamus is indirectly responsible for pituitary development and function.

otx2b $^{hu3625/hu3625}$ have mandible and eye defects

In humans, whole gene deletions and heterozygous mutations of *OTX2* are associated with mandibular anomalies including micrognathia and agnathia and ocular defects such as

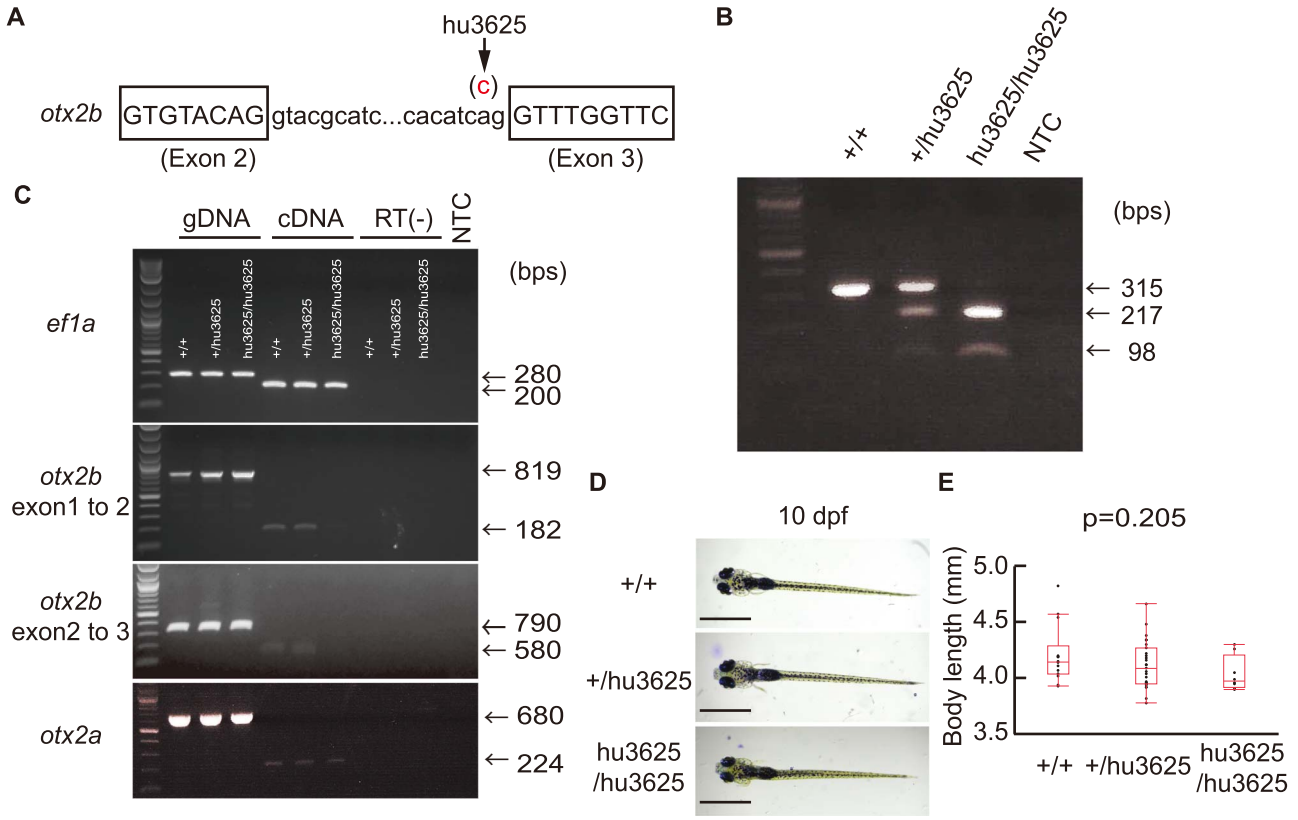

Figure 1. The *otx2b*$^{hu3625/hu3625}$ mutant fish have no functional *otx2b* transcripts. (**A**) *otx2b*^{hu3625} variant is an A to C mutation in an invariant part of the splice acceptor site upstream of exon 3. (**B**) The *otx2b*^{hu3625} mutation introduces an MspI digestion site within the mutant allele. The uncut WT product measures 315 bp, while the *otx2b*^{hu3625} product is cleaved by MspI into 217 bp and 98 bp fragments. (**C**) *Otx2b*$^{hu3625/hu3625}$ homozygous fish had no detectable *otx2b* cDNA transcripts prior to the mutated splice site (exon 1–2) or containing the mutated splice site (exon 2–3). *otx2a* cDNA transcripts Genomic DNA produced the expected size bands for WT (+/+), heterozygotes (+/hu3625) and homozygotes (hu3625/hu3625). The detection of *ef1a* was used as an internal control. (**D** and **E**) Representative images and median measurement of body length at 10 dpf demonstrated no difference between +/+, heterozygotes (+/hu3625) and homozygotes (hu3625/hu3625). Sample numbers are 14 WT, 27 heterozygotes and 8 homozygotes.

Table 1. *otx2b*$^{hu3625/hu3625}$ zebrafish show early death before 13 dpf. Genotype distribution from the intercross of heterozygous *otx2b*$^{+/hu3625}$ zebrafish matings

Age of assessment	Analyzed number	Number [+/+]–[+/hu3625]–[hu3625/hu3625]	% [+/+]–[+/hu3625]–[hu3625/hu3625]
1 dpf	269	69–136—64	25.7–50.6—23.8
2 dpf	125	30–58—37	24.0–46.4—29.6
3 dpf	306	70–161—75	22.9–52.6—24.5
5 dpf	528	125–257—146	23.7–48.7—27.7
10 dpf	614	167–312—135	27.2–50.8—22.0
13 dpf	86	27–59—0	31.4–68.6—0
2 months	167	66–101—0	39.5–60.5—0

dpf = days post fertilization.

microphthalmia, anophthalmia and coloboma. Using the jaw index, which is the ratio of jaw to head size (22), the 10 dpf *otx2b*$^{hu3625/hu3625}$ mutant larvae demonstrated a modest, but statistically significant reduction in mandible size in contrast to other genotypes (only 3.4% reduction from WT, Fig. 3A and B). In addition, 10 dpf *otx2b*$^{hu3625/hu3625}$ mutant larvae showed small eyes (67.6 ± 11.7% size of WT, Fig. 3C and D, Supplementary Fig. S3A–C). Methylacrylate sections at 3 and 10 dpf confirmed a microphthalmic eye that showed disorganization of the neural layers of the retina in *otx2b*$^{hu3625/hu3625}$ mutant larvae (Fig. 3E and F) (23). However, optokinetic reflex response to evaluate oculomotor and visual function demonstrated no differences between genotypes, indicating that the mutant larvae can at least detect gross motion (data not shown). We hypothesized that decreased vision contributed to early death of *otx2b*$^{hu3625/hu3625}$ larvae because visual acuity is important for finding food after nutrition from the yolk is exhausted. The requirement for food intake coincides with lethality of *otx2b*$^{hu3625/hu3625}$ larvae at ∼11 dpf. Intake of fluorescent food at 7 and 10 dpf was scored qualitatively as 'positive', in which the entire stomach was fluorescent, 'minimal', in which only a trace of food was in the stomach, and 'negative'. At 10 dpf, the majority of *otx2b*$^{hu3625/hu3625}$ mutant larvae was negative for food intake, 16.7% had a trace of food, and none was

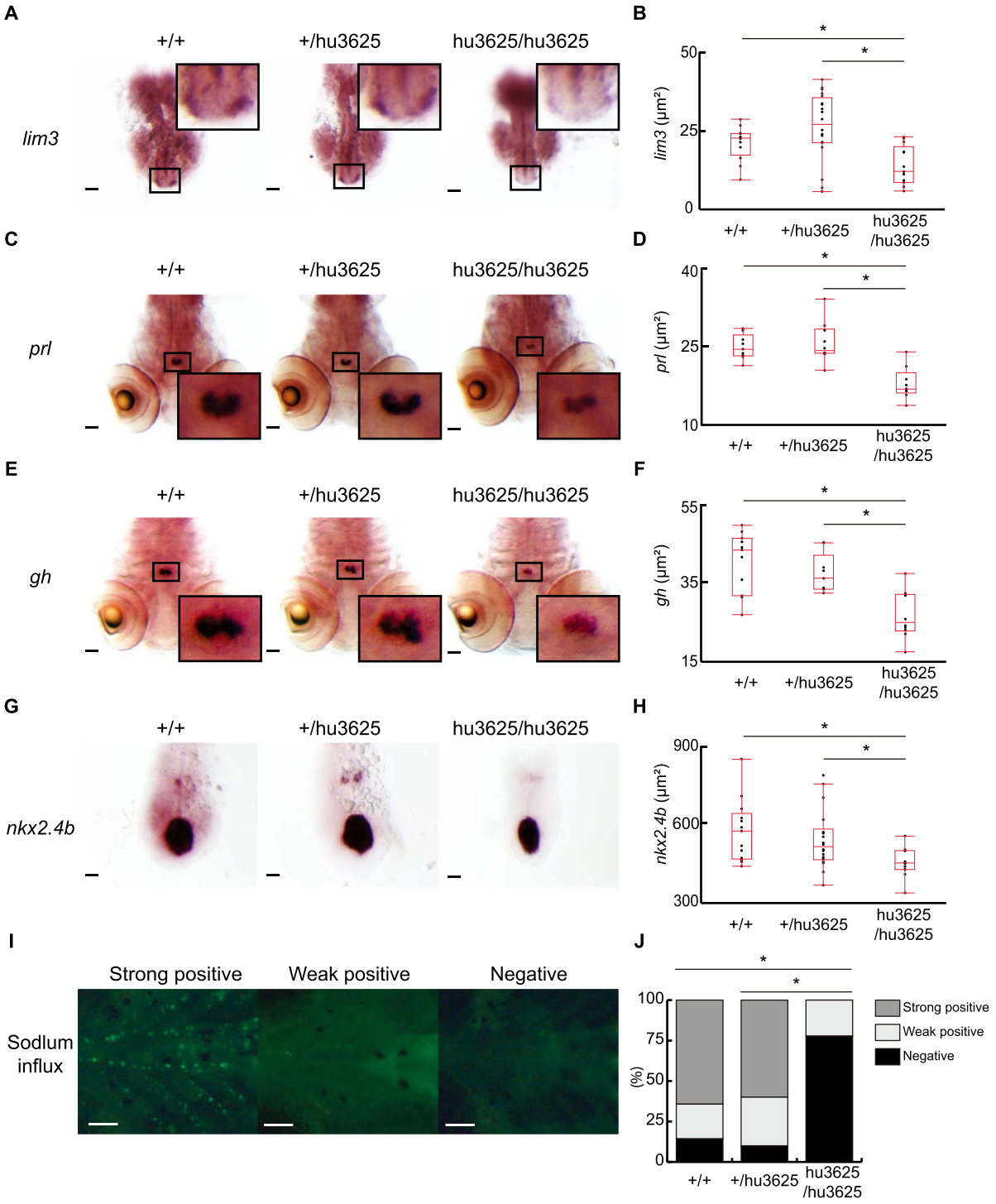

Figure 2. *otx2b*$^{hu3625/hu3625}$ have decreased areas of pituitary hormone expression. (**A** and **B**) Whole-mount *in situ* hybridization (A) and median area of distribution (B) at 1 dpf of *lim3* demonstrated decreased expression in homozygotes (hu3625/hu3625) in contrast to WT (+/+) and heterozygotes (+/hu3625). Sample numbers are 12 WT, 20 heterozygotes and 13 homozygotes. (**C–F**) Whole-mount *in situ* hybridization and median area of distribution at 10 dpf of *prl* (C and D) and *gh* (E and F) demonstrated decreased expression in homozygotes. Sample numbers of *prl* and *gh* are 9 WT, 11 heterozygotes and 9 homozygotes and 11 WT, 10 heterozygotes and 9 homozygotes, respectively. (**G** and **H**) Whole-mount *in situ* hybridization (G) and median area of distribution at 1 dpf (H) of *nkx2.4b* demonstrated decreased expression in homozygotes. Sample numbers are 13 WT, 18 heterozygotes and 11 homozygotes. (**I** and **J**) Homozygotes showed a higher percentage of larvae in contrast to WT and heterozygotes with decreased sodium accumulation within the gills (J), which was graded positive, weak positive and negative (I). Sample numbers are 14 WT, 30 heterozygotes and 9 homozygotes. (Scale:10 μm).

positive (Fig. 3G and H). To control for the possibility that *otx2b*$^{hu3625/hu3625}$ are not well enough to eat food attributable to other physiological problems, we performed the food intake experiment with 7 dpf fish (Supplementary Fig. S3D and E). Seven dpf *otx2b*$^{hu3625/hu3625}$ larvae were also negative for food accumulation, indicating that the mutants had impaired vision

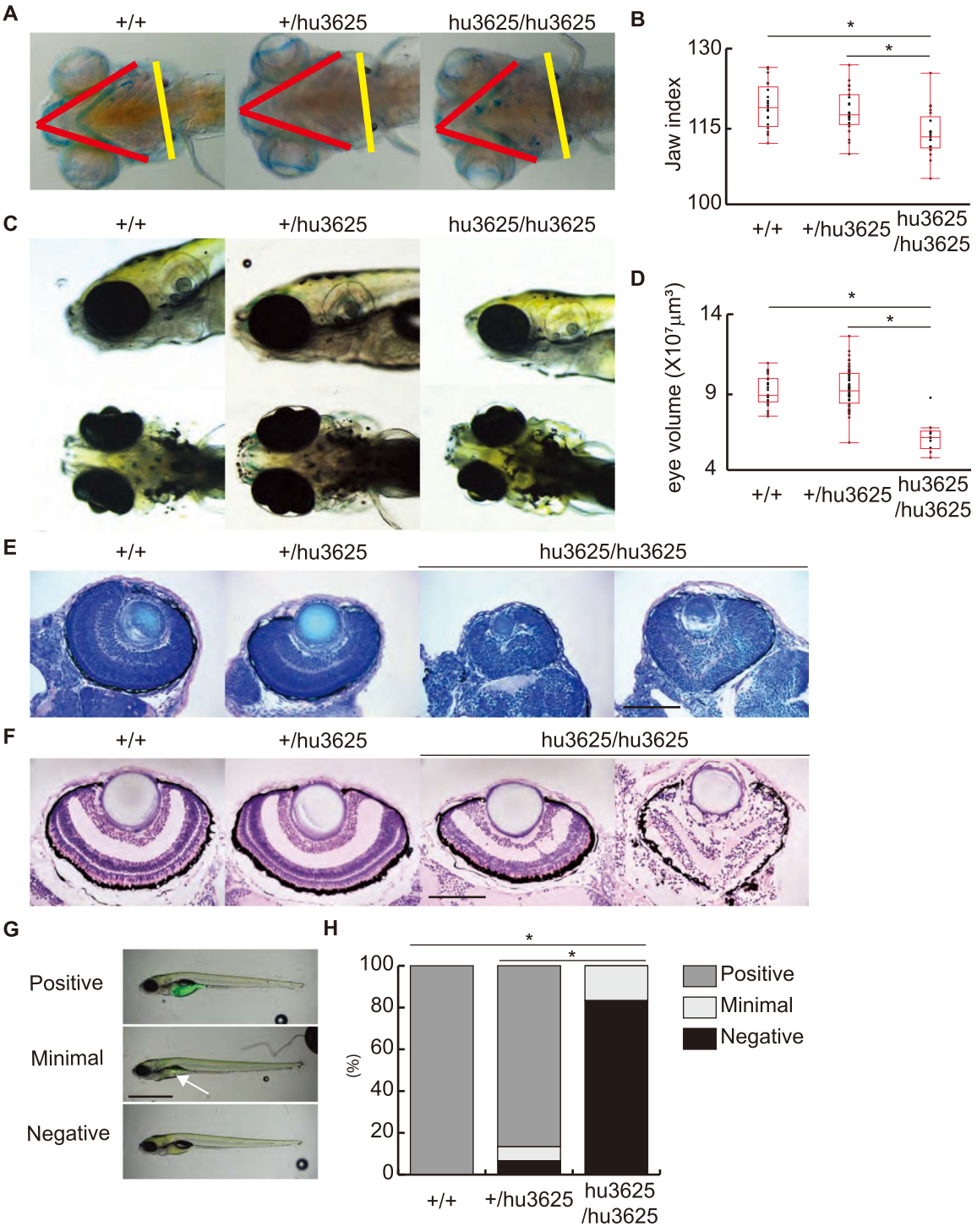

Figure 3. *otx2b*$^{hu3625/hu3625}$ displayed mandible and ocular defects similar to human variants. (**A** and **B**) Alcian blue cartilage staining at 10 dpf. (A) demonstrated smaller mandibles as calculated by the median jaw index [B, (left jaw length (red line) + right jaw length)/2)/head transverse diameter (yellow line) × 100] in the homozygotes (hu3625/hu3625) in contrast to WT (+/+) and heterozygotes (+/hu3625). Sample numbers are 20 WT, 22 heterozygotes and 20 homozygotes. (**C** and **D**) External images of 10 dpf larvae (C) demonstrate decreased anterior-posterior and dorsal-ventral eye size and reduced median eye volume (D) in homozygotes (hu3625/hu3625) in contrast to WT (+/+) and heterozygotes (+/hu3625). Sample numbers are 23 WT, 64 heterozygotes and 10 homozygotes. (**E** and **F**) Methylacrylate sections at 3 dpf (E) demonstrated impaired differentiation and disorganization of the neural retina in homozygotes in contrast to WT and heterozygotes. At 10 dpf (F) some homozygotes showed the loss of retinal architecture and integrity. (**G**) food intake was graded 'positive', 'minimal' and 'negative'. (**H**) Homozygotes showed a significantly lower percentage of larvae at 10 dpf in contrast to WT and heterozygotes with poor food intake. Sample numbers are 7 WT, 15 heterozygotes and 12 homozygotes.

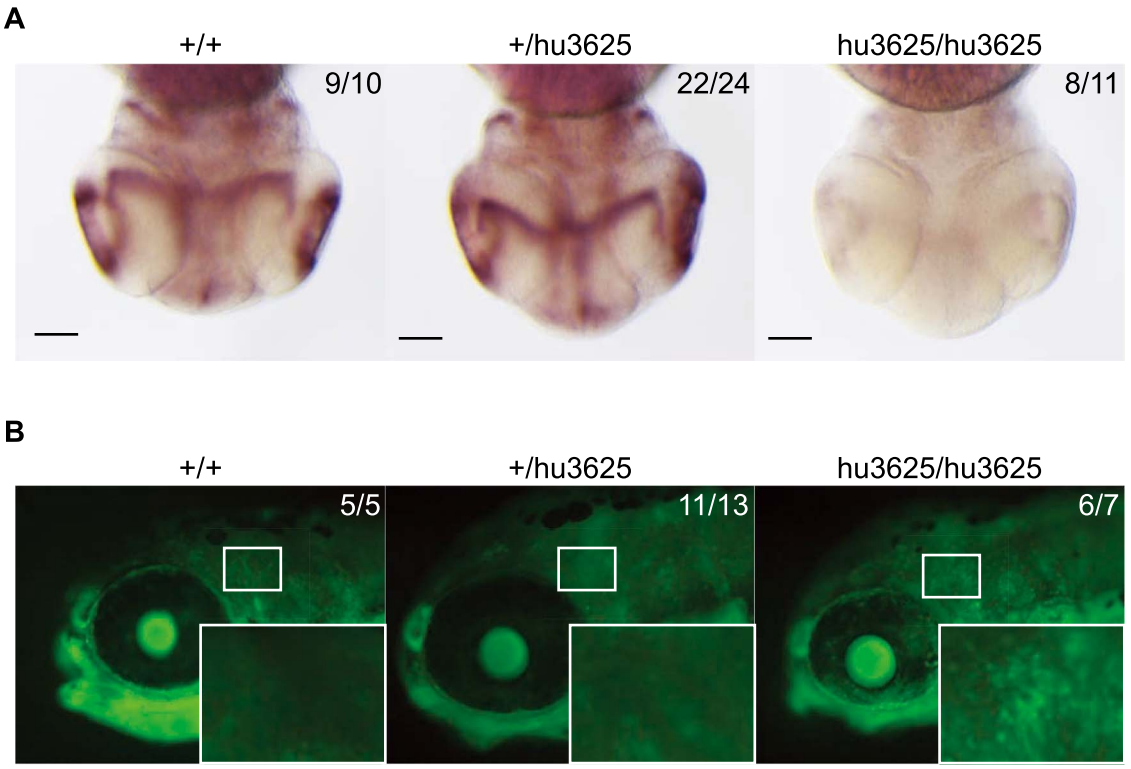

Figure 4. *otx2b*$^{hu3625/hu3625}$ shows low cell proliferation and high apoptosis in the head. (**A**) Whole-mount *in situ* hybridization of PCNA demonstrated decreased cell proliferation in 3 dpf homozygotes (hu3625/hu3625) in contrast to WT (+/+) and heterozygotes (+/hu3625). (**B**) Acridine orange staining at 5 dpf revealed increased apoptosis within the head region in homozygotes (hu3625/hu3625) in contrast to WT (+/+) and heterozygotes (+/hu3625).

and did not have other physiologic problems that prevented food intake.

Reduced cell proliferation and elevated apoptosis in the developing head of *otx2b* deficient zebrafish

Since *otx2b*$^{hu3625/hu3625}$ mutants have small pituitary, mandible and eyes, we hypothesized that decreased cell proliferation and increased apoptosis underlie the hypoplasia of these organs. *In situ* hybridization for proliferating cell nuclear antigen (PCNA) showed decreased staining in the head and eye region in *otx2b*$^{hu3625/hu3625}$ at 3 dpf (Fig. 4A), but not 1 dpf (data not shown). Acridine orange staining to assess for apoptosis demonstrated accumulation in the heads of *otx2b*$^{hu3625/hu3625}$ mutants but not in WT or *otx2b*$^{hu3625/+}$ at 5 dpf (Fig. 4B). No differences were noted between genotypes at either 1 or 3 dpf (data not shown). Thus, organ hypoplasia in the *otx2b*$^{hu3625/hu3625}$ mutants was associated with decreased cell proliferation and increased apoptosis in the forebrain and midbrain.

Discussion

Homozygous *otx2b* mutant zebrafish have striking defects in pituitary and eye development and modest changes in mandible development. These structures are also affected in humans and rodents with heterozygous loss-of-function alleles, indicating the conservation of gene function across vertebrates. However, heterozygous *otx2b* zebrafish are phenotypically normal, indicating a difference in dosage sensitivity between fish and mammals. This could be attributable to *otx2a*, the paralogue of *otx2b*, which may partially compensate the loss of *otx2b* function. In the current studies, *otx2b* mutant fish were analyzed as (i) *otx2b* morphants exacerbate the morphant phenotype of other genes that regulate eye and jaw development (2), (ii) a functional study with fugu fish (*Takifugu niphobles*) showed only *otx2b* functions as a head organizer gene (24), (iii) *otx2b* has a higher degree of homology with the mammalian *Otx2* gene in contrast to *otx2a* and (iv) the Otx2b protein was registered as a homologous to the OTX2 protein in other species. Thus, despite the differences between mammals and zebrafish, the mutant zebrafish are a useful tool for analyzing the functional significance of rare, likely deleterious mutations in *OTX2* that are identified in human patients.

In the current studies, *otx2b*$^{hu3625/hu3625}$ mutant larvae showed microphthalmic eyes with disorganization of the neural retina. This resulted in abnormal vision, which likely led to difficulty in finding food after the yolk sac is depleted (~6–7 dpf) and eventual starvation and early mortality around 11 dpf. In humans, *OTX2* mutations are associated with the microphthalmia-anophthalmia-coloboma spectrum and can lead to varying degrees of visual impairment and in some cases complete blindness. In mice, *in vitro* gene expression analysis suggests that *Otx2*, in coordination with *Sox2* (25), is a direct upstream regulator of *Rax*. Like *OTX2*, human mutations in *retina and anterior neural fold homeobox (Rax)* or its homolog in mice (*Rx1*) and zebrafish (*rx3*) are also associated with microphthlamia, anophthalmia and coloboma, indicting an important signaling pathway in eye development.

In mammals, OTX2 is a known regulator of pituitary development and its function. Similarly, in the current studies, we found that in zebrafish *otx2b* was required for anterior pituitary development. However, since *otx2b* expression was not

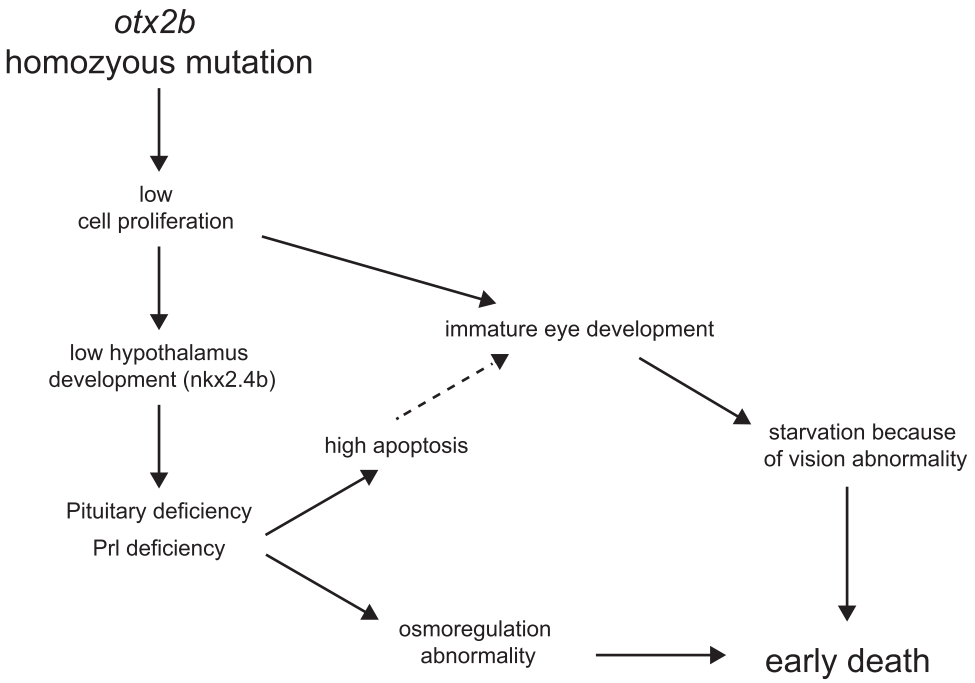

Figure 5. Proposed mechanism of small pituitary, eye and mandibular and early death of *otx2b*$^{hu3625/hu3625}$.

detected in the pituitary itself, the gene acted indirectly through the hypothalamus, which was found to be small with reduced *nkx2.4b* and *fgf3* expression in *otx2b*$^{hu3625/hu3625}$ mutants. This parallels the mechanistic findings in mice, in which selective disruption of *Otx2* in the mouse neural ectoderm and subsequent ventral diencephalon causes anterior pituitary hypoplasia with poor development of the infundibulum and stalk and decreased FGF signaling (8). In mouse neural crest development, OTX2 protein is translocated to cells that do not express it (26). We cannot exclude the possibility that Otx2b protein translocates from non-pituitary tissue to the developing pituitary gland.

Otx2b was also required for pituitary function as *otx2b*$^{hu3625/hu3625}$ mutants showed decreased expression of *lim3*, zebrafish orthologue of *Lhx3* and reduced expression of *prl* and *gh*. Reduced *prl*, which controls several ion transporters and regulates osmotic homeostasis in zebrafish (20), led to decreased ion intake, without obvious edema, in *otx2b*$^{hu3625/hu3625}$ mutants. More drastic reductions in *prl* action, such as *prl* mutant zebrafish or MO-knockdown of *prl* receptors, causes a more profound phenotype including dysregulation of sodium, potassium and chloride homeostasis and obvious edema and death between 6 and 16 dpf. Taken together, this suggests that the reduced expression of *prl* alters osmoregulation and may contribute to the early death of the *otx2b*$^{hu3625/hu3625}$ mutant larvae (Fig. 5).

The *otx2b*$^{hu3625/hu3625}$ mutant zebrafish exhibited both high apoptosis and low cell proliferation in the developing head, which contributed to the hypoplasia of multiple craniofacial structures. In different mouse models, *Otx2* knockout also demonstrated alterations in proliferation and apoptosis, although not within the same tissue. For example, hypothalamus-specific *Otx2* knockout mice exhibited reduced proliferation, but no obvious cell death (7), whereas photoreceptor-specific *Otx2* knockout mice had increased apoptosis but not reduced cell proliferation (27). Further, human induced pluripotent stem cells carrying a clinically significant *OTX2* variant showed increased apoptosis when differentiated into a pituitary cell fate (28). The differences in cell death and proliferation may be tissue and species dependent, but also may be attributable to the timing of experiments related to development and animal death.

In conclusion, we demonstrate that homozygous loss of *otx2b* in zebrafish affects development of the hypothalamus, pituitary gland, mandible and eye. Because *otx2b* is expressed in the neural ectoderm, and not the oral ectoderm, the hypopituitarism of *otx2b* mutant zebrafish is secondary to hypothalamic hypoplasia. We show the utility of mutant zebrafish for the functional analysis of *OTX2* and other human CPHD-related genes that are associated with a broad variety of phenotypes.

Materials and Methods

Zebrafish

All the procedures were performed under the University of Michigan University Committee on the Use and Care of Animals guidelines. Zebrafish were maintained under standard temperature (28.5°C) and light cycle conditions (14 h on, 10 h off). The supplementation of larval fish food started at 5 dpf. *Otx2b* mutant fish (*otx2b*^{hu3625}) on an AB background were generated by the Zebrafish Mutation Project at the Wellcome Sanger Institute using ethyl-N-nitrosourea mutagenesis and commercially obtained from Zebrafish International Resource Center (ZIRC, University of Oregon, Eugene, OR, USA).

Genotyping

DNA was extracted from caudal fin tissue amputated from fish anesthetized with tricaine (Sigma-Aldrich) by using TNES buffer (10 mM Tris pH 7.5, 400 mM NaCl, 100 mM ethylenediaminetetraacetic acid (EDTA) and 0.6% sodium dodecyl sulfate (SDS)) with proteinase K (PK), followed by co-precipitation with 6 M

NaCl, precipitation with 100% EtOH, and re-suspension with TE buffer. DNA extraction from larvae after taking the photos for blinded experiments were extracted by the following solution; 50 mM Tris–HCl pH 8.0, 0.5% Tween-20, and 800 μg/ml PK. After overnight incubation, samples were incubated at 95°C for 15 min and added as PCR template. A 315 base pair (bp) fragment containing the mutation-induced MspI cleavage site was amplified by PCR using the primer pair (forward/reverse): 5′-cgtgtacaggtacgcatctttcaactc-3′/5′-gctcttctttttggcaggtcgcacc-3′ and the following amplification parameters: 95°C for 3 min; 35 cycles of 95°C for 30 s, 57°C for 30 s and 72°C for 30 s; and 72°C for 4 min. The PCR products were incubated at 37°C with MspI for 1 h and then separated by gel electrophoresis. The PCR product for the WT allele was 315 bp, whereas the restriction enzyme digestion of the hu3625 allele resulted in 217 bp and 98 bp fragments (Fig. 1B).

Measurement of larval size

Five and 10 dpf zebrafish larvae were anesthetized in tricaine and then mounted in 3% methyl cellulose for live imaging on a stereo microscope, which was calibrated with a stage micrometer slide. The genotypes of larvae were blinded until after larval size data were collected.

RNA extraction and RT-PCR

Total RNAs were extracted from 5 dpf sample with TRIzol Reagent (Invitrogen) following standard protocols (29). Reverse transcription was performed with SuperScript First-Strand Synthesis System for RT-PCR (Invitrogen). Primer sets were as follows (forward/reverse): *ef1a* (5′-caagcccatgtgtgtggaga-3′/5′-atcaagaagagtagtaccgctagcattac-3′), *otx2b* exon 1–2 (5′-acggtcaacgggctaagttt-3′/5′-acctcctcgcgcatgaaaat-3′), *otx2b* exon 2–3(5′-aatcaacttgccggagtccc-3′/5′- tttccatgaggacgcttggt-3′) and *otx2a* (5′-atacctcaagcaggccccgta-3′/5′-gcaaattaatcttcagggcgacc-3′).

Whole-mount *in situ* hybridization

Whole-mount RNA *in situ* hybridization was performed following standard protocols (30). Briefly, embryos/larvae were fixed with 4% paraformaldehyde (PFA) in phosphate-buffered saline (PBS) and hydrated by 100% methanol at −20°C. After bringing samples to room temperature, samples were incubated in 50% methanol and washed with PBS with 0.1% Tween (PBST). Samples older than 24 hpf were bleached with 3% hydrogen peroxide (H_2O_2) and 0.5% potassium hydroxide (KOH). PK digestion in Tris–EDTA was performed, following blocking of endogenous alkaline phosphatase (AP) with 0.1 M triethanolamine in 0.25% acetic anhydride. Samples were pre-hybridized for 1 h and then incited with the denatured anti-sense RNA probes overnight at 56°C. Samples were washed with serial solutions; 50% formamide with 1X saline–sodium citrate buffer (SSC), 2X SSC, 0.2X SSC, 0.1X SSC with PBST and PBST. Samples were incubated with blocking reagent (Roche) and then anti-DIG-AP (1:5000, Roche) overnight at 4°C. Samples were washed several times with PBST and then developed with 5-bromo-4-chloro-3-indolyl-phosphate/nitro blue tetrazolium (Roche) in 0.1 M TRIS pH 9.5/0.1 M $NaCl_2$ and 0.05 M $MgCl_2$ overnight. Samples were washed with PBS-T and 4% PFA-PBS and stored in 100% glycerol. Images were obtained on a concave slide, followed by genotyping. The pictures of each median data are shown in the figures. *In situ* hybridization probes were a gift of Dr Matthias Hammerschmidt. The PCNA probes were kindly provided by Dr Alessandro Cellerino (31).

Acridine orange staining

Acridine orange staining for detecting apoptosis was performed as previously reported (32, 33). Briefly, larvae were incubated in the dark for 30 min at room temperature in acridine orange solution (2 μg/ml, Sigma, A9231), followed by washing 4 times for 5 min each in fish water. Larvae were anesthetized, mounted in 3% methylcellulose and visualized with a fluorescence stereo microscope.

Eye histology

Zebrafish larvae were fixed in 2% PFA/1.5% glutaraldehyde overnight at 4°C and then embedded in methylacrylate. Blocks were section at 5 μm and mounted on slides. Staining with Lee's stain was performed using standard techniques (34). Permanent coverslips were placed using mounting medium (CytoSeal; Richard-Allan Scientific, Kalamazoo, MI).

Cartilage and bone staining

Cartilage and bone staining were performed as previously reported with modification (35). Briefly, after fixation with formaldehyde/PBS, cartilage was stained with alcian blue solution (70 μl 0.4% alcian blue/70% ethanol + 925 μl 95% ethanol + 55 μl 1 M $MgCl_2$) for 4 h. After discarding the alcian blue solution, samples were washed with 95% ethanol. Bone was stained by alizarin red solution (10 μl 0.5% alizarin red/water + 990 μl 95% ethanol) for 2 days. Following cartilage and bone staining, samples were bleached with 1.5% H_2O_2 + 1% KOH. Bleached samples were cleared by 20% glycerol with 0.25% KOH and store in 50% glycerol and 0.1% KOH at 4°C. The jaw index was calculated as previously reported (22); Jaw index = [(left jaw length + right jaw length)/2]/head transverse diameter × 100.

Food intake test

Food intake test were performed as previously reported with a small modification (36). Briefly, fertilized eggs were collected and housed in about 50 ml of embryo medium in 10 cm Petri dishes. Larvae were trained to feed by sprinkling the medium in each dish with 2 mg of powdered larval fish food from 4 to 9 dpf. The larvae were allowed to feed for 3–4 h and then transferred to a clean Petri dish containing fresh embryo medium. Fluorescent food is a dried mixture of 150 μl of yellow–green (505/515) fluorospheres (F8827, Invitrogen, Carlsbad, CA), 50 μl of deionized water, and 100 mg of powdered larval food. On 7 or 10 dpf, powdered fluorescent food was fed to the larvae in the same manner as during the training period. The larvae were allowed to feed on fluorescent food for 2 h, mounted in 3% methyl cellulose, and imaged with a fluorescent stereomicroscope. We classified the food intake level as enough, by chance level and none. After imaging, the larvae were harvested for DNA extraction and genotyping.

Sodium influx analysis

Sodium influx was analyzed using sodium green staining (37). Briefly, 7 dpf larvae were incubated in 10 μM sodium green tetraacetate (S6901, Invitrogen) in fish water for 1 h. Subsequently, larvae were washed with fish water. Larvae were anesthetized with tricaine, mounted in 3% methyl cellulose, and the

accumulation of fluorescent sodium in the gills was visualized using a fluorescence stereomicroscope. Larvae were then harvested for DNA extraction and genotyping. We divided the level of sodium influx into three categories: strong positive, weak positive and negative.

Image analysis

Images of cartilage and bone staining, eye size, food intake test, acridine orange staining and sodium influx analysis were obtained with a DFC310 FX Digital Color Camera (Leica Microsystems, Wetzlar, Germany) and were processed using LasX software (Leica Microsystems). The smaller sized eyes were used for calculation of the eyes. Images of whole mount *in situ* hybridization were obtained with DS-Ri1 (Nikon, Tokyo, Japan) and were processed using ViewNX 2 (Nikon). Data were analyzed using Fiji software (38).

Statistical analysis

Statistical analyses were performed using JMP Statistical Database Software version 12.2.0 (SAS Institute, Cary, NC). Analysis of variance, Wilcoxon signed-rank test and Fisher's exact test were used as appropriate. A P-value of < 0.05 was considered statistically significant.

Supplementary Material

Supplementary Material is available at *HMG* online.

Acknowledgment

We thank Natasha Golovchenko, Sierra S. Nishizaki and Anthony Antonellis (Department of Human Genetics, University of Michigan Medical School), and Queena Zhao, Allison Ferguson and Hao Hao Pontius (Division of Pediatric Hematology/Oncology, Department of Pediatrics, University of Michigan) for managing the fish system. We thank Brad Nelson for tissue processing, sectioning and staining of the methyl acrylate ocular sections. We thank Antionette L. Williams and Phillip E. Kish (Department of Ophthalmology and Visual Sciences, Kellogg Eye Center, University of Michigan) and laboratory members for their fruitful suggestions.

Conflict of Interest statement: None declared.

Funding

National Institutes of Health (R01 30428 to S.A.C.; R01 HL124232, and R01 HL125774 to J.A.S.); the Japan Society for the Promotion of Science Overseas Research Fellowship, the Japan Society (to H.B.); Vision Research Core (P30 EY007003 to B.N.) from the National Eye Institute, Department of Ophthalmology and Visual Sciences, Kellogg Eye Center, University of Michigan.

References

1. Simeone, A., Acampora, D., Gulisano, M., Stornaiuolo, A. and Boncinelli, E. (1992) Nested expression domains of four homeobox genes in developing rostral brain. *Nature*, **358**, 687–690.
2. Chassaing, N., Sorrentino, S., Davis, E.E., Martin-Coignard, D., Iacovelli, A., Paznekas, W., Webb, B.D., Faye-Petersen, O., Encha-Razavi, F., Lequeux, L. *et al.* (2012) OTX2 mutations contribute to the otocephaly-dysgnathia complex. *J. Med. Genet.*, **49**, 373–379.
3. Ragge, N.K., Brown, A.G., Poloschek, C.M., Lorenz, B., Henderson, R.A., Clarke, M.P., Russell-Eggitt, I., Fielder, A., Gerrelli, D., Martinez-Barbera, J.P. *et al.* (2005) Heterozygous mutations of OTX2 cause severe ocular malformations. *Am. J. Hum. Genet.*, **76**, 1008–1022.
4. Dateki, S., Kosaka, K., Hasegawa, K., Tanaka, H., Azuma, N., Yokoya, S., Muroya, K., Adachi, M., Tajima, T., Motomura, K. *et al.* (2010) Heterozygous orthodenticle homeobox 2 mutations are associated with variable pituitary phenotype. *J. Clin. Endocrinol. Metab.*, **95**, 756–764.
5. Fang, Q., George, A.S., Brinkmeier, M.L., Mortensen, A.H., Gergics, P., Cheung, L.Y., Daly, A.Z., Ajmal, A., Perez Millan, M.I., Ozel, A.B. *et al.* (2016) Genetics of combined pituitary hormone deficiency: roadmap into the genome era. *Endocr. Rev.*, **37**, 636–675.
6. Hide, T., Hatakeyama, J., Kimura-Yoshida, C., Tian, E., Takeda, N., Ushio, Y., Shiroishi, T., Aizawa, S. and Matsuo, I. (2002) Genetic modifiers of otocephalic phenotypes in Otx2 heterozygous mutant mice. *Development*, **129**, 4347–4357.
7. Mortensen, A.H., Schade, V., Lamonerie, T. and Camper, S.A. (2015) Deletion of OTX2 in neural ectoderm delays anterior pituitary development. *Hum. Mol. Genet.*, **24**, 939–953.
8. Herzog, W., Sonntag, C., von der Hardt, S., Roehl, H.H., Varga, Z.M. and Hammerschmidt, M. (2004) Fgf3 signaling from the ventral diencephalon is required for early specification and subsequent survival of the zebrafish adenohypophysis. *Development*, **131**, 3681–3692.
9. Sbrogna, J.L., Barresi, M.J. and Karlstrom, R.O. (2003) Multiple roles for hedgehog signaling in zebrafish pituitary development. *Dev. Biol.*, **254**, 19–35.
10. Herzog, W., Sonntag, C., Walderich, B., Odenthal, J., Maischein, H.M. and Hammerschmidt, M. (2004) Genetic analysis of adenohypophysis formation in zebrafish. *Mol. Endocrinol.*, **18**, 1185–1195.
11. Dutta, S., Dietrich, J.E., Aspock, G., Burdine, R.D., Schier, A., Westerfield, M. and Varga, Z.M. (2005) pitx3 defines an equivalence domain for lens and anterior pituitary placode. *Development*, **132**, 1579–1590.
12. Nica, G., Herzog, W., Sonntag, C. and Hammerschmidt, M. (2004) Zebrafish pit1 mutants lack three pituitary cell types and develop severe dwarfism. *Mol. Endocrinol.*, **18**, 1196–1209.
13. Stainier, D.Y.R., Raz, E., Lawson, N.D., Ekker, S.C., Burdine, R.D., Eisen, J.S., Ingham, P.W., Schulte-Merker, S., Yelon, D., Weinstein, B.M. *et al.* (2017) Guidelines for morpholino use in zebrafish. *PLoS Genet.*, **13**, e1007000.
14. Kettleborough, R.N., Busch-Nentwich, E.M., Harvey, S.A., Dooley, C.M., de Bruijn, E., van Eeden, F., Sealy, I., White, R.J., Herd, C., Nijman, I.J. *et al.* (2013) A systematic genome-wide analysis of zebrafish protein-coding gene function. *Nature*, **496**, 494–497.
15. El-Brolosy, M.A., Kontarakis, Z., Rossi, A., Kuenne, C., Gunther, S., Fukuda, N., Kikhi, K., Boezio, G.L.M., Takacs, C.M., Lai, S.L. *et al.* (2019) Genetic compensation triggered by mutant mRNA degradation. *Nature*, **568**, 193–197.
16. Schilter, K.F., Schneider, A., Bardakjian, T., Soucy, J.F., Tyler, R.C., Reis, L.M. and Semina, E.V. (2011) OTX2 microphthalmia syndrome: four novel mutations and delineation of a phenotype. *Clin. Genet.*, **79**, 158–168.

17. Matsuo, I., Kuratani, S., Kimura, C., Takeda, N. and Aizawa, S. (1995) Mouse Otx2 functions in the formation and patterning of rostral head. *Genes Dev.*, **9**, 2646–2658.
18. Davis, S.W., Castinetti, F., Carvalho, L.R., Ellsworth, B.S., Potok, M.A., Lyons, R.H., Brinkmeier, M.L., Raetzman, L.T., Carninci, P., Mortensen, A.H. *et al.* (2010) Molecular mechanisms of pituitary organogenesis: in search of novel regulatory genes. *Mol. Cell. Endocrinol.*, **323**, 4–19.
19. Pogoda, H.M. and Hammerschmidt, M. (2007) Molecular genetics of pituitary development in zebrafish. *Semin. Cell Dev. Biol.*, **18**, 543–558.
20. Shu, Y., Lou, Q., Dai, Z., Dai, X., He, J., Hu, W. and Yin, Z. (2016) The basal function of teleost prolactin as a key regulator on ion uptake identified with zebrafish knockout models. *Sci. Rep.*, **6**, 18597.
21. Uhlen, M., Fagerberg, L., Hallstrom, B.M., Lindskog, C., Oksvold, P., Mardinoglu, A., Sivertsson, A., Kampf, C., Sjostedt, E., Asplund, A. *et al.* (2015) Proteomics. Tissue-based map of the human proteome. *Science*, **347**, 1260419.
22. Paladini, D., Morra, T., Teodoro, A., Lamberti, A., Tremolaterra, F. and Martinelli, P. (1999) Objective diagnosis of micrognathia in the fetus: the jaw index. *Obstet. Gynecol.*, **93**, 382–386.
23. Richardson, R., Tracey-White, D., Webster, A. and Moosajee, M. (2017) The zebrafish eye-a paradigm for investigating human ocular genetics. *Eye (Lond.)*, **31**, 68–86.
24. Kurokawa, D., Ohmura, T., Akasaka, K. and Aizawa, S. (2012) A lineage specific enhancer drives Otx2 expression in teleost organizer tissues. *Mech. Dev.*, **128**, 653–661.
25. Danno, H., Michiue, T., Hitachi, K., Yukita, A., Ishiura, S. and Asashima, M. (2008) Molecular links among the causative genes for ocular malformation: Otx2 and Sox2 coregulate Rax expression. *Proc. Natl. Acad. Sci. U. S. A.*, **105**, 5408–5413.
26. Sugiyama, S., Di Nardo, A.A., Aizawa, S., Matsuo, I., Volovitch, M., Prochiantz, A. and Hensch, T.K. (2008) Experience-dependent transfer of Otx2 homeoprotein into the visual cortex activates postnatal plasticity. *Cell*, **134**, 508–520.
27. Nishida, A., Furukawa, A., Koike, C., Tano, Y., Aizawa, S., Matsuo, I. and Furukawa, T. (2003) Otx2 homeobox gene controls retinal photoreceptor cell fate and pineal gland development. *Nat. Neurosci.*, **6**, 1255–1263.
28. Matsumoto, R., Suga, H., Aoi, T., Bando, H., Fukuoka, H., Iguchi, G., Narumi, S., Hasegawa, T., Muguruma, K., Ogawa, W. *et al.* (2020) Congenital pituitary hypoplasia model demonstrates hypothalamic OTX2 regulation of pituitary progenitor cells. *J. Clin. Invest.*, **130**, 641–654.
29. Peterson, S.M. and Freeman, J.L. (2009) RNA isolation from embryonic zebrafish and cDNA synthesis for gene expression analysis. *J. Vis. Exp.*, 1470.
30. Westerfield, M. (2000) *The Zebrafish Book. A Guide for the Laboratory Use of Zebrafish (Danio rerio)*, 4th edn. University of Oregon Press, Eugene.
31. Baumgart, M., Groth, M., Priebe, S., Savino, A., Testa, G., Dix, A., Ripa, R., Spallotta, F., Gaetano, C., Ori, M. *et al.* (2014) RNA-seq of the aging brain in the short-lived fish N. furzeri - conserved pathways and novel genes associated with neurogenesis. *Aging Cell*, **13**, 965–974.
32. Harris, M.P., Rohner, N., Schwarz, H., Perathoner, S., Konstantinidis, P. and Nusslein-Volhard, C. (2008) Zebrafish eda and edar mutants reveal conserved and ancestral roles of ectodysplasin signaling in vertebrates. *PLoS Genet.*, **4**, e1000206.
33. Hu, Z., Liu, Y., Huarng, M.C., Menegatti, M., Reyon, D., Rost, M.S., Norris, Z.G., Richter, C.E., Stapleton, A.N., Chi, N.C. *et al.* (2017) Genome editing of factor X in zebrafish reveals unexpected tolerance of severe defects in the common pathway. *Blood*, **130**, 666–676.
34. Prophet, E.B., Millis, B., Arrington, J.B. and Sobin, L.H. (1992) *Laboratory Methods in Histotechnology*. American Registry of Pathology, Washington, DC.
35. Walker, M.B. and Kimmel, C.B. (2007) A two-color acid-free cartilage and bone stain for zebrafish larvae. *Biotech. Histochem.*, **82**, 23–28.
36. Cassar, S., Huang, X. and Cole, T. (2018) High-throughput measurement of gut transit time using larval Zebrafish. *J. Vis. Exp.*, **140**, doi: 10.3791/58497.
37. Esaki, M., Hoshijima, K., Kobayashi, S., Fukuda, H., Kawakami, K. and Hirose, S. (2007) Visualization in zebrafish larvae of Na(+) uptake in mitochondria-rich cells whose differentiation is dependent on foxi3a. *Am. J. Physiol. Regul. Integr. Comp. Physiol.*, **292**, R470–R480.
38. Schindelin, J., Arganda-Carreras, I., Frise, E., Kaynig, V., Longair, M., Pietzsch, T., Preibisch, S., Rueden, C., Saalfeld, S., Schmid, B. *et al.* (2012) Fiji: an open-source platform for biological-image analysis. *Nat. Methods*, **9**, 676–682.